Test of the anisotropy method for Lamb-shift measurements—theory and experiment*

G. W. F. Drake,† P. S. Farago,‡ and A. van Wijngaarden
Department of Physics, University of Windsor, Windsor, Ontario, Canada
(Received 3 December 1974)

We show that a measurement of the anisotropy in the angular distribution of the quenching radiation emitted by metastable hydrogen and deuterium atoms in an electric field can be used to determine the Lamb shift to an accuracy of at least ±0.1%. The method can be extended to the hydrogenic ions, where it offers several advantages over the quench-rate technique used in earlier measurements. The experiment is interpreted by means of a nonperturbative theory of the quenching process, which includes hyperfine structure and time-dependent effects. In the limit of zero field strength, the anisotropies of H and D are measured to be 0.139 01 ± 0.000 12 and 0.141 21 ± 0.000 14, while the theoretical values are 0.139 078 and 0.141 30, respectively. The corresponding Lamb shifts are 1057.3 ± 0.9 MHz and 1058.7 ± 1.1 MHz.

I. INTRODUCTION

In previous papers,[1,2] we have suggested that a measurement of the anisotropy in the angular distribution of the Ly α radiation, emitted by metastable hydrogenic $2s_{1/2}$ ions in an electric field, may provide an accurate method of determining Lamb shifts. A measurement of the anisotropy is completely equivalent to previous polarization measurements,[3,4] but for technical reasons the anisotropy can be measured much more accurately. The method offers several advantages over the extensively used quench-rate technique.[5-8] For example, the field strength need not be known as accurately since the effect is independent of field strength in the limit of weak fields. Also, a single measurement at one optimum point along the ion beam is sufficient; it is not necessary to track the intensity over several decay lengths with the consequent loss of intensity and uncertainties introduced by beam bending.

The purpose of this paper is to provide a precision test of the technique in hydrogen and deuterium where the Lamb shift is accurately known from microwave resonance measurements.[9,10] Our earlier results[2] suffered from a number of systematic errors which have since been eliminated by redesigning the equipment. The high accuracy of the results provides an interesting test of the nonperturbative quenching theory developed by one of us.[11] The application of the quenching theory to hydrogen and deuterium is described in Sec. II, and the experiment is discussed in Sec. III.

II. THEORY

In this section, the nonperturbative theory discussed in a separate paper[11] (denoted by I) is applied to the Stark quenching of hydrogen and deuterium.

The process to be described is shown schematically in Fig. 1. A hydrogen atom in one of its four possible $2s_{1/2}$ hyperfine states is injected into an electric field. The field induces mixing with the twelve possible intermediate $2p_{1/2}$ and $2p_{3/2}$ states, each of which can radiate to the $1s_{1/2}$ ground state. We assume that the field is not so strong as to cause significant mixing with higher np states, but it is otherwise arbitrary. Also, hyperfine structure in the ground state and ground-state perturbations can safely be neglected due to the large $2p$-$1s$ energy separation.

Using the notation of I, the time dependence of the field is assumed to have the form

$$V(\vec{r},t)=\lim_{\epsilon\to+0}\mathcal{F}V(\vec{r})e^{-\epsilon t}\,,\quad t\geq 0$$
$$=0,\quad t<0 \qquad (1)$$

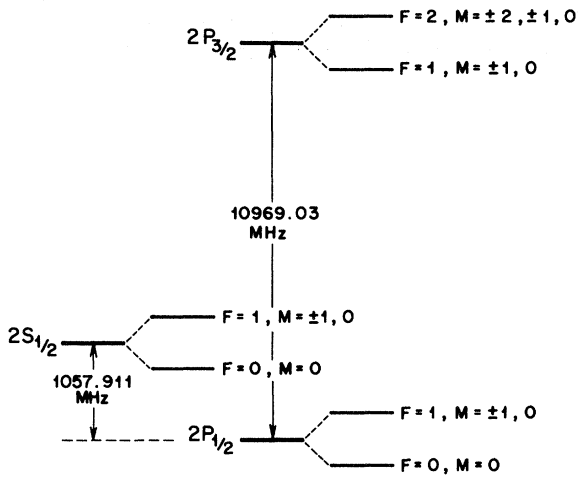

FIG. 1. Energy-level diagram for the $n=2$ states of hydrogen. The hyperfine splitting of the $2s_{1/2}$ state is 177.567 MHz. Virtual transitions from the $2s$ states to the $2p$ states are followed by radiative transitions to the ground state.

with $V(\vec{r}) = -ez$ and $\mathcal{F}$ is the field strength. In the subspace of the four $2s$ states and twelve $2p$ states, the interaction matrix $\underline{V}$ has the off-diagonal form

$$\underline{V} = \begin{pmatrix} 0 & \underline{V}_{sp} \\ \underline{V}_{ps} & 0 \end{pmatrix}. \tag{2}$$

For a problem of this type, it is shown in I that the exact time-dependent Green's function relating the state of the atom at a time $t_2 < 0$ to the state of the atom at a time $t_1 > 0$ is

$$G^+(\vec{r}_1 t_1; \vec{r}_2 t_2) = \frac{1}{2\pi i} \int_{-\infty}^{\infty} d\omega_1 \, e^{i\omega_1 t_1} \underline{\psi}^\dagger(\vec{r}_2, t_2) \underline{g}(\omega_1) \underline{\psi}(\vec{r}_1), \tag{3}$$

where, in the finite basis set, $\underline{\psi}^\dagger(\vec{r}_2, t_2)$ is the 16-component row vector of field-free s and p eigenstates, and $\underline{\psi}(\vec{r}_1)$ is the Hermitian-conjugate column vector without the time-dependent phase factors $e^{-iE_n t}$. The submatrix $\underline{g}_{sp}(\omega_1)$ of the frequency response matrix $\underline{g}(\omega_1)$ determines the properties of the field-induced radiation. It is given by (see I. 44 in the limit $\epsilon_j \to 0$)

$$\underline{g}_{sp}(\omega_1) = -\mathcal{F} \det(\underline{\Delta}_{pp}) \underline{D}_{ss}^{-1} \underline{V}_{sp} \underline{\Delta}_{pp}^{-1}, \tag{4}$$

where

$$\underline{D}_{ss} = \det(\underline{\Delta}_{pp})(\underline{\Delta}_{ss} - \underline{V}_{sp} \underline{\Delta}_{pp}^{-1} \underline{V}_{ps} \mathcal{F}^2), \tag{5}$$

$\underline{\Delta}_{pp}$ is a diagonal matrix in the subspace of p states with diagonal-matrix elements $\Delta_{np} = E_{np} + \omega_1$, and n is an index labeling the twelve $2p$ states. $\underline{\Delta}_{ss}$ is defined similarly. Equation (4) is the matrix generalization to an arbitrary number of states of the two-state results found by Fontana and Lynch.[12]

$\underline{D}_{ss}$ is an $N_s \times N_s$ matrix, where N_s is the number of s states. If the z axis is chosen to lie along the electric-field direction, then $\underline{D}_{ss}$ is block diagonalized according to the value of the magnetic quantum number M_F, where $\vec{F} = \vec{J} + \vec{I}$ is the total angular momentum. Since $J = \frac{1}{2}$ for the s states, at most two states can have the same value of M_F. Therefore, the inversion of $\underline{D}_{ss}$ in (4) reduces to the inversion of at most a 2×2 matrix for any nuclear spin I. For the hydrogen atom, $I = \frac{1}{2}$ and $F = 0, 1$. $\underline{D}_{ss}^{-1}$ is therefore

$$\underline{D}_{ss}^{-1} = \det(\underline{\Delta}_{pp})^{-1} \begin{pmatrix} \underline{d}^{(0)} & 0 & 0 \\ 0 & \underline{d}^{(1)} & 0 \\ 0 & 0 & \underline{d}^{(-1)} \end{pmatrix}, \tag{6}$$

where the superscripts are the values of M_F. The elements $\underline{d}^{(\pm 1)}$ are 1×1 matrices given by

$$d^{(m)} = \frac{\det(\underline{\Delta}_{pp}^{(m)})}{\prod_k (-\beta_k^{(m)} + \omega_1)}, \quad m = \pm 1, \tag{7}$$

and the $\beta_k^{(m)}$ are the negatives of the eigenvalues of the matrix $(\underline{E} + \mathcal{F}\underline{V})$ in the subspace of s and p states with $M_F = m$. $\underline{E}$ is the diagonal matrix of field-free eigenvalues, $E_n - \frac{1}{2} i \Gamma_n$, including fine and hyperfine structure, and $\underline{\Delta}_{pp}^{(m)}$ is the diagonal submatrix of $\underline{\Delta}_{pp}$ in the space of p states with $M_F = m$. The remaining element $\underline{d}^{(0)}$ is a 2×2 matrix of the form

$$\underline{d}^{(0)} = \begin{pmatrix} d_{\mu\mu}^{(0)} & d_{\mu\nu}^{(0)} \\ d_{\nu\mu}^{(0)} & d_{\nu\nu}^{(0)} \end{pmatrix}, \tag{8}$$

where μ denotes the state $2s_{1/2}$ ($F = 0$, $M_F = 0$) and ν denotes the state $2s_{1/2}$ ($F = 1$, $M_F = 0$). The matrix elements are

$$d_{\mu\mu}^{(0)} = \frac{\det(\underline{\Delta}_{pp}^{(0)})}{\prod_k (-\beta_k^{(0)} + \omega_1)} \left(\Delta_\nu - \mathcal{F}^2 \sum_n \frac{V_{\nu n} V_{n\nu}}{\Delta_{np}} \right), \tag{9}$$

$$d_{\mu\nu}^{(0)} = \frac{\det(\underline{\Delta}_{pp}^{(0)})}{\prod_k (-\beta_k^{(0)} + \omega_1)} \left(\mathcal{F}^2 \sum_n \frac{V_{\nu n} V_{n\mu}}{\Delta_{np}} \right), \tag{10}$$

together with the corresponding two equations with μ and ν interchanged. The results are written in the above form to make the poles and residues of $\underline{g}_{sp}(\omega_1)$ immediately obvious.

To calculate the properties of the field-induced radiation, we assume that the initial state is an incoherent mixture of all four $2s_{1/2}$ hyperfine states with equal statistical weights. The matrix elements of $\underline{V}$ between hyperfine states are easily evaluated by standard vector-coupling techniques[13] in terms of 3-j and 6-j symbols. Using Eqs. I.60 and I.61, together with the above expressions for the matrix elements of $\underline{g}_{sp}$, the expression for the time-dependent transition rate integrated over all frequencies, summed over the final $1s$ hyperfine states, and averaged over initial states, can be written in the form

$$I(\hat{e}, t) = 2\pi\hbar\rho(\bar{\omega}) \tfrac{1}{4} |H'_{2p,1s}|^2 [|\hat{e} \cdot \hat{F}|^2 |A(t)|^2 + |\hat{e} \times \hat{F}|^2 |A'(t)|^2], \tag{11}$$

where $\hat{e}$ is the unit polarization vector of the emitted photon and $\hat{F}$ is a unit vector in the direction of the electric field. $H'_{2p,1s}$ is the $2p$-$1s$ electric-dipole radiative-transition integral given by

$$H'_{2p,1s} = e \left(\frac{2\pi\hbar\bar{\omega}}{\mathcal{V}} \right)^{1/2} \frac{\hbar^2}{me^2} \frac{2^7\sqrt{2}}{3^5}, \tag{12}$$

and $\rho(\bar{\omega})$ is the density of photon states $(\hbar\bar{\omega})^2 \mathcal{V}/(2\pi\hbar c)^3$ per unit energy at the average frequency $\bar{\omega} \simeq (E_{2s} - E_{1s})/\hbar$. $A(t)$ and $A'(t)$ are lengthy expressions resulting from summing the residues of $\underline{g}_{sp}(\omega_1)$ over its poles as shown in Eq. I.61. The contributions can be classified according to the hyperfine-structure quantum numbers F, M, and

F', M' of the initial and final states, respectively. Thus

$$|A(t)|^2 = \mathcal{F}^2 \sum_{F,M,F'} \left| \sum_k e^{i\beta_k^{(M)} t} \mathrm{Res}[B^{F,M}_{F',M'}(\omega_1)]_{\omega_1=\beta_k^{(M)}} \right|^2 \tag{13}$$

with $M'=M$. The corresponding expression for $|A'(t)|^2$ is the same except that $M'=M-1$. The $B^{F,M}_{F',M'}$ have the form

$$B^{F,M}_{F',M'}(\omega_1) = \frac{\det(\underline{\Delta}^{(M)}_{pp})}{\prod_j(-\beta_j^{(M)}+\omega_1)} C^{F,M}_{F',M'}(\omega_1) . \tag{14}$$

Let the np states be labeled by $n=1,\ldots,4$ in the order $2p_{1/2}(F=0)$, $2p_{1/2}(F=1)$, $2p_{3/2}(F=1)$, $2p_{1/2}(F=2)$. For $M=\pm 1$, the C's in (14) are

$$C^{F,\pm 1}_{F',M'}(\omega_1) = \sum_{n=2}^{4} \frac{\alpha_n}{\Delta_n} \tag{15}$$

with the nonvanishing coefficients α_n given in Table I. For $M=0$, the C's have the more complicated structure

$$C^{F,0}_{F',M'}(\omega_1) = \sum_{n=1}^{4} \frac{\alpha_n}{\Delta_n} \left(\Delta_{2s_{1/2}(F\pm 1)} - 3\mathcal{F}^2 \sum_{n'=1}^{4} \frac{\beta^{(F)}_{n,n'}}{\Delta_{n'}} \right) \tag{16}$$

with the coefficients $\beta^F_{n,n'}$ listed in Table II and the α_n in Table I. The sign is to be chosen to that $F\pm 1$ is 0 or 1.

The corresponding results for deuterium, which has $I=1$, can be expressed in a similar form. In this case there are five p states to be considered, labeled by n in the order $2p_{1/2}(\frac{1}{2})$, $2p_{1/2}(\frac{3}{2})$, $2p_{3/2}(\frac{1}{2})$, $2p_{3/2}(\frac{3}{2})$, $2p_{3/2}(\frac{5}{2})$. The coefficients α_n and $\beta^{(F)}_{n,n'}$ to be used in (15) and (16) are given in Tables III and IV. The sign in (16) is to be chosen so that $F\pm 1$ is $\frac{1}{2}$ or $\frac{3}{2}$. For both hydrogen and deuterium, the results for the case $I=0$ are recovered by neglecting the hyperfine-structure energy splittings.

The experimentally measured quantity is the

TABLE I. Values of the coefficients α_n in Eqs. (15) and (16) for hydrogen.

$C^{F,M}_{F',M'}$ \ n	1	2	3	4
$C^{0,0}_{0,0}$	0	1	2	0
$C^{1,0}_{1,0}$	1	0	0	2
$C^{1,\pm 1}_{1,\pm 1}$	0	1	$\frac{1}{2}$	$\frac{3}{2}$
$C^{0,0}_{1,\pm 1}$	0	∓ 1	± 1	0
$C^{1,\pm 1}_{0,0}$	0	∓ 1	± 1	0
$C^{1,\pm 1}_{1,0}$	1	$\frac{1}{2}$	$-\frac{3}{2}$	0
$C^{1,0}_{1,\pm 1}$	1	0	0	-1

TABLE II. Values of the coefficients $\beta^{(F)}_{n,n'}$ in Eq. (16) for hydrogen with $F=0,1$.

n \ n'	1	2	3	4
1	0	1	2	0
2	1	0	0	2
3	1	0	0	2
4	0	1	2	0

total intensity summed over both polarizations emitted in directions parallel and perpendicular to the electric field. Summing (11) over two perpendicular vectors $\hat{e}$, both perpendicular to the direction of propagation, yields

$$I(\theta,\varphi,t) = 2\pi\hbar\rho(\bar{\omega})^{\frac{1}{4}} |H'_{2p,1s}|^2 \times \{ |A(t)|^2[\sin^2\varphi + \cos^2\theta\cos^2\varphi] + |A'(t)|^2[\sin^2\varphi + (1+\sin^2\theta)\cos^2\varphi] \} , \tag{17}$$

where θ, φ are the spherical angles defining the direction of propagation and $\hat{F}$ is taken to point in the x direction. The anisotropy is defined by

$$R = \frac{I_\parallel - I_\perp}{I_\parallel + I_\perp} , \tag{18}$$

where $I_\parallel = I(\frac{1}{2}\pi, 0, t)$ and $I_\perp = I(\theta, \frac{1}{2}\pi, t)$. Thus from (17),

TABLE III. Values of the coefficients α_n in Eqs. (15) and (16) for deuterium. The upper and lower signs are to be taken together.

$C^{F,M}_{F',M'}$ \ n	1	2	3	4	5
$C^{1/2,\pm 1/2}_{1/2,\pm 1/2}$	$\frac{1}{9}$	$\frac{8}{9}$	$\frac{8}{9}$	$\frac{10}{9}$	0
$C^{1/2,\pm 1/2}_{3/2,\pm 1/2}$	$\mp\frac{1}{9}\sqrt{8}$	$\pm\frac{1}{9}\sqrt{8}$	$\pm\frac{1}{9}\sqrt{8}$	$\mp\frac{1}{9}\sqrt{8}$	$\pm\frac{1}{5}\sqrt{8}$ [a]
$C^{3/2,\pm 1/2}_{1/2,\pm 1/2}$	$\mp\frac{1}{9}\sqrt{8}$	$\pm\frac{1}{9}\sqrt{8}$	$\pm\frac{1}{9}\sqrt{8}$	$\mp\frac{1}{9}\sqrt{8}$	0
$C^{3/2,\pm 1/2}_{3/2,\pm 1/2}$	$\frac{8}{9}$	$\frac{1}{9}$	$\frac{1}{9}$	$\frac{4}{45}$	$\frac{27}{15}$
$C^{3/2,\pm 3/2}_{3/2,\pm 3/2}$	0	1	0	$\frac{4}{5}$	$\frac{6}{5}$
$C^{1/2,\pm 1/2}_{1/2,\mp 1/2}$	$\frac{1}{9}\sqrt{2}$	$-\frac{4}{9}\sqrt{2}$	$\frac{8}{9}\sqrt{2}$	$-\frac{5}{9}\sqrt{2}$	0
$C^{1/2,\pm 1/2}_{3/2,\mp 1/2}$	$\mp\frac{2}{9}$	$\pm\frac{8}{9}$	$\pm\frac{2}{9}$	$\mp\frac{8}{9}$	$\mp\frac{2}{5}$ [a]
$C^{1/2,\pm 1/2}_{3/2,\pm 3/2}$	$\mp\frac{2}{9}\sqrt{3}$	$\mp\frac{4}{9}\sqrt{3}$	$\pm\frac{2}{9}\sqrt{3}$	$\pm\frac{4}{9}\sqrt{3}$	$\pm\frac{2}{15}\sqrt{3}$ [a]
$C^{3/2,\pm 1/2}_{1/2,\mp 1/2}$	$\mp\frac{4}{9}$	$\mp\frac{2}{9}$	$\pm\frac{4}{9}$	$\pm\frac{2}{9}$	0
$C^{3/2,\pm 3/2}_{1/2,\pm 1/2}$	0	$\mp 2/\sqrt{3}$	0	$\pm 2/\sqrt{3}$	0
$C^{3/2,\pm 1/2}_{3/2,\mp 1/2}$	$\frac{4}{9}\sqrt{2}$	$\frac{2}{9}\sqrt{2}$	$\frac{1}{18}\sqrt{2}$	$\frac{8}{45}\sqrt{2}$	$-\frac{9}{10}\sqrt{2}$
$C^{3/2,\pm 1/2}_{3/2,\pm 3/2}$	$\frac{4}{9}\sqrt{6}$	$-\frac{2}{9}\sqrt{6}$	$\frac{1}{18}\sqrt{6}$	$\frac{4}{45}\sqrt{6}$	$-\frac{3}{10}\sqrt{6}$
$C^{3/2,\pm 3/2}_{3/2,\pm 1/2}$	0	$\frac{1}{3}\sqrt{6}$	0	$\frac{4}{15}\sqrt{6}$	$-\frac{3}{5}\sqrt{6}$

[a] For these terms, the contribution from $\Delta_{2s_{1/2}(F\pm 1)}$ in (16) is to be omitted.

$$R=\frac{|A'(t)|^2-|A(t)|^2}{3|A'(t)|^2+|A(t)|^2}. \tag{19}$$

It follows directly from (11) that the polarization in a direction perpendicular to $\hat{F}$ is

$$P=\frac{|A(t)|^2-|A'(t)|^2}{|A(t)|^2+|A'(t)|^2}. \tag{20}$$

Combining (19) and (20) yields

$$P=2R/(R-1) \tag{21}$$

independent of time and field strength. Thus, measurements of P and R are completely equivalent and yield identical information. The total instantaneous decay rate is obtained by integrating (17) over all angles.

The interference terms in (13) resulting from the sum over k lead to rapid oscillations over times comparable to the lifetime of the $2p$ state. The oscillations result from the sudden switching on of the field and will not be present unless the field is actually switched on sufficiently rapidly.[14] In this experiment, the field is switched on over a period of a few nanoseconds, which is fast compared to the lifetime of the $2s$ state, but slow compared to the lifetime of the $2p$ state. The oscillations in (13) can be suppressed and the long-time behavior of the radiation obtained by retaining in the sum over k only those poles $\beta_k^{(M')}$ correlating with s states, since they have small imaginary parts if the field is not too strong (greater than several hundred V/cm). The p-type poles, which produce the oscillations, have large imaginary parts and do not contribute after several p-state lifetimes. For hydrogen, the oscillations in R obtained by omitting the $2p_{3/2}$ $(F=1,2)$ poles and retaining the $2s_{1/2}$ $(F=0,1)$ and $2p_{1/2}$ $(F=0,1)$ poles in the sum over k are shown in Fig. 2. The rapid oscillations at approximately the Lamb-shift frequency are modulated at the hyperfine frequency of the $2s_{1/2}$ state. Except for the modulation, similar results were obtained by Macek.[14] It is clear that the oscillating curve tends asymptotically to the smooth curve calculated by retaining only the four $2s_{1/2}$ $(F=0,1)$ poles. Since the experimental results were taken at times larger than 20 nsec, we adopt the procedure of retaining only the s-type poles in the calculations. The resulting anisotropy is still weakly time-dependent due to the slightly different depopulation rates of different hyperfine states as shown in Fig. 5. The smooth curve is the same as in Fig. 2, but drawn to a different scale. Also, the partial hyperfine-structure uncoupling by the external field is accounted for. However, the results are incorrect for very short times where the details of switching on the field are important.

TABLE IV. Values of the coefficients $\beta_{n,n'}^{(F)}$ in Eq. (16) for deuterium.

n \ n'	1	2	3	4	5
		$F=\frac{1}{2}$			
1	0	1	1	$-\frac{4}{5}$	$\frac{9}{5}$
2	1	0	0	$\frac{1}{5}$	$\frac{9}{5}$
3	1	0	0	$\frac{1}{5}$	$\frac{9}{5}$
4	$\frac{4}{5}$	$\frac{1}{5}$	$\frac{1}{5}$	0	$\frac{9}{5}$
5	1	−1	−1	1	0
		$F=\frac{3}{2}$			
1	0	1	1	1	0
2	1	0	0	2	0
3	1	0	0	2	0
4	−1	2	2	0	0
5	$\frac{1}{9}$	$\frac{8}{9}$	$\frac{8}{9}$	$\frac{10}{9}$	0

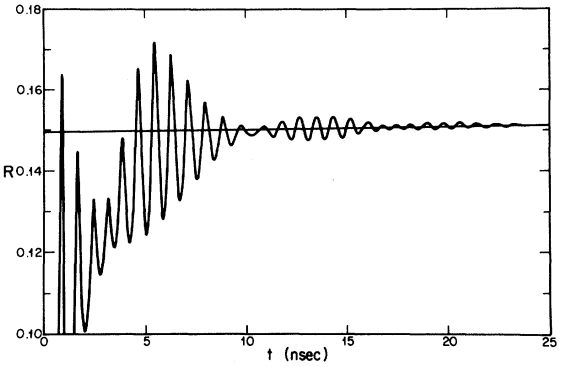

FIG. 2. Theoretical calculation of the anisotropy R for hydrogen as a function of elapsed time after entering the field of strength 151.6 V/cm. The smooth curve is the same as that shown in Fig. 5 on a different scale.

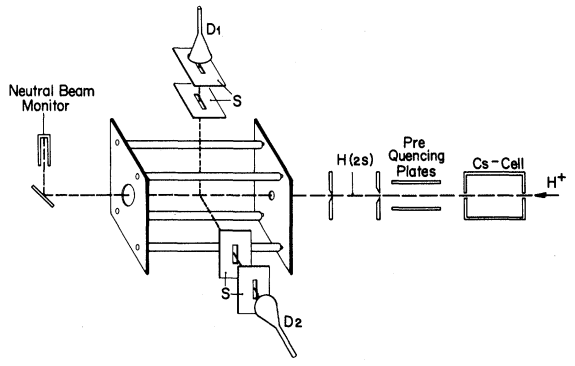

FIG. 3. Diagram of the apparatus. An outer conducting cylinder held at ground potential surrounding the quadrupole rods is not shown.

III. DESCRIPTION OF THE EXPERIMENT

A schematic drawing of the apparatus is shown in Fig. 3. In summary, a monoenergetic beam of typically 10-keV H^+ or D^+ ions enters a cell containing Cs vapor. The emerging beam contains[15,16] neutral atoms, protons, H^-, and an intense component of the desired metastable $H(2s)$ atoms, whose field-free lifetime is 0.14 sec. To reduce background noise, a small electric field (~10 V/cm) is applied between the prequenching plates to remove charged particles from the beam. The remaining beam is collimated and then enters the quadrupole electric-quenching-field region. Here the induced photons emitted in two directions are counted simultaneously by a double-counter system, and the beam current is recorded by a neutral-particle detector. The various components are described in somewhat greater detail below.

The near-resonant charge-exchange reaction[16]

$$H^+ + Cs \rightarrow [H(2s), H(2p)] + Cs^+ - 0.49 \text{ eV}$$

occurs with high efficiency when the proton beam passes through the cesium cell. The $H(2p)$ component decays rapidly, leaving only the $H(2s)$ component a few millimeters downstream from the cell, along with ground-state atoms and ions. With a cesium cell length of 10 cm, the optimum $H(2s)$ current of about 10^{10} particles/sec in the observation region is obtained with a cell temperature of about 100 °C. The cell entrance and exit slits (0.1 cm×0.6 cm) are maintained at a higher temperature to prevent the accumulation of Cs metal. Before entering the quadrupole, the beam is collimated to an angular divergence of 0.4°, giving a beam 0.15 cm in diameter at the position of the detectors.

The quadrupole system is constructed from four symmetrically placed rods held in position between two grounded metal plates by insulating glass balls. The rods are connected together in two *nearest*-neighbor pairs with the two pairs held at opposite potentials. The rods are surrounded by a conducting cylinder held at ground potential to provide a well-defined boundary condition for the field inside. The quadrupole rods 0.762 cm in diameter and 8.636 cm long are located on a circle of diameter 3.302 cm. The diameter of the outer cylinder is 6.99 cm. The field at the beam axis is due to the large dipole moment of the system and for our geometry is very nearly constant across the beam diameter. This system has several advantages: (i) observations can easily be made from all four sides; (ii) the field direction can be rotated in steps of $\frac{1}{2}\pi$ by switching potentials; and (iii) the field, including the rod diameter and end effects, can be calculated to any prescribed accuracy by expanding the solution as an infinite sum of solutions to Laplace's equation of appropriate symmetry in cylindrical coordinates. In performing the calculation, the total region inside the outer cylinder held at zero potential is divided into inner and outer regions by an imaginary cylinder of inversion symmetry passing through the rods. Only the regular radial solution contributes in the inner region, while both regular and irregular solutions contribute in the outer regions such that $V=0$ on the outer cylinder and end plates, and V is continuous across the boundary. The first n-expansion coefficients are determined by demanding that V be a constant on the rods and dV/dr be continuous across the boundary at n points.

The ultraviolet photon detectors D_1 and D_2 (Galileo Electro-Optics model BX 762) have a quantum efficiency of about 10% for Ly α radiation, while the dark noise does not exceed 0.5 counts/sec. With two detectors, the effects of beam fluctuations are eliminated.

IV. ANALYSIS OF ERRORS

In addition to corrections for background noise and finite solid angles of observation, there are two main effects which can introduce an instrumental asymmetry: (a) the two detectors have somewhat different acceptance angles and detection efficiencies; (b) the presence of stray magnetic fields, $\vec{B}$, give rise to a motional electric field $(1/c)\vec{v}\times\vec{B}$. Both these effects can be eliminated to a high degree of accuracy by rotating the quenching field in steps of $\frac{1}{2}\pi$ in the plane perpendicular to the beam. This is achieved by a cyclic change in polarity of the quadrupole rods. The counting rates $N_1(\varphi)$ and $N_2(\varphi+\frac{1}{2}\pi)$ of the two detectors are measured simultaneously at each of the four consecutive field orientations $\varphi = 0, \frac{1}{2}\pi, \pi, \frac{3}{2}\pi$.

The effect of stray fields is reduced to a negligible second-order correction by forming the average quantities

$$N_1' = \tfrac{1}{2}[N_1(0)+N_1(\pi)], \tag{22}$$

$$N_2' = \tfrac{1}{2}[N_2(\tfrac{1}{2}\pi)+N_2(\tfrac{3}{2}\pi)], \tag{23}$$

$$N_1'' = \tfrac{1}{2}[N_1(\tfrac{1}{2}\pi)+N_1(\tfrac{3}{2}\pi)], \tag{24}$$

$$N_2'' = \tfrac{1}{2}[N_2(0)+N_2(\pi)]. \tag{25}$$

The efficiencies and acceptance angles of the detectors as well as beam fluctuations are then eliminated by forming

$$r^2 = (N_1' N_2'')/(N_2' N_1''), \tag{26}$$

which is related to the apparent anisotropy R' by

$$R' = (r-1)/(r+1). \tag{27}$$

This must still be corrected for background noise and the finite solid angle of observation. The background noise was measured by applying a high (1500 V/cm) prequenching field to destroy the metastables and determining the *isotropic* component of the still observable radiation with the same quenching field. (A small anisotropic component persists due to the subsequent creation of new metastables in the beam downstream from the prequenching region.) The neutral beam current was monitored with the aid of a current-to-frequency converter to define an effectively constant counting period for the signal and noise measurements, independent of beam fluctuations. The noise thus defined was subtracted from the $N_j(\varphi)$ in (22)–(25). As a check, the corrected values remained statistically unchanged when the noise was deliberately varied from 0.5% to 10% of the signal.

The solid-angle correction is obtained by integrating (17) over the solid angle seen by each detector. The effect is small because the geometrical dependence of the counting rate on acceptance angle has already been eliminated by the use of (26). The residual effect resulting from averaging R over the range of angles seen by the detectors is particularly small for φ near $\frac{1}{2}n\pi$. For our geometry, it increases R by the factor 1.0027. The precise dimensions of the two slit systems are, therefore, not of critical importance and need not even be the same to a high degree of precision.

The remaining sources of error are statistical fluctuations, and uncertainties in the dimensions and alignment of the quadrupole system. Assuming that the standard deviation in a total of N_j counts is $\pm\sqrt{N_j}$, the statistical uncertainty $\pm\delta R$ in R is

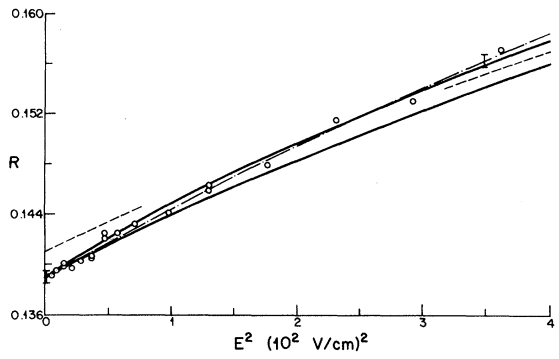

FIG. 4. Comparisons of the experimental and theoretical anisotropies for hydrogen as a function of E^2 (E is the field strength). The dot-dash curve is the quadratic least-squares fit to the individual measurements shown by circles. The lower solid curve is the theory, including hyperfine structure, at $t=0$ and the upper solid curve is the theory at $t=25$ nsec. The dashed curve is the theory without hyperfine structure.

$$\delta R \simeq 2\sqrt{r}/[(r+1)\sqrt{N}] \tag{28}$$

where N is the total number of counts registered by both detectors. The most accurate single measurements contain about 3×10^7 counts to give a statistical uncertainty in R of about 0.15%. This dominates our estimates of the geometrical and alignment uncertainties and is the major source of error.

V. RESULTS

The anisotropy R (corrected for noise and finite solid angle of observation) was measured at a sequence of different quenching-field strengths $\mathcal{F}$ and a curve

$$R=\sum_{k=0}^{n} a_k\mathcal{F}^{2k}$$

was fitted to the experimental results. In performing the least-squares fit to single runs, the approximation to $n=2$ was always found to be statistically significant. The coefficient a_0 gives the zero-field anisotropy independent of the field-strength calibration or errors dependent on powers of $\mathcal{F}^2$. The Lamb shift Δ_L is obtained by calculating R as a function of Δ_L for a particular value of $\mathcal{F}$ using the method described in Sec. II.

Figure 4 shows the results obtained in a typical run with metastable hydrogen at a velocity of 1.1×10^8 cm/sec. The statistical error for each measured point is the same and is indicated by one error bar. The dot-dash line is the least-squares fit and the error bar at $\mathcal{F}=0$ is the computed standard deviation σ_{ext} in the extrapolated value R ($\mathcal{F}=0$). The statistical accuracy of the central value is taken to be $\pm\sigma_{\text{ext}}/\sqrt{N}$, where $N=19$ is the number of points on the curve. The two solid curves represent the theoretical calculations obtained with the input data in Table V. The lower curve is the theory at $t=0$ (without the effects produced by p-type poles) and the upper curve is calculated for a transit time between entering the field and reaching the detectors of 25 nsec appropriate

TABLE V. Input data for theoretical calculations of R.

	Hydrogen	Deuterium
$E(2s_{1/2})-E(2p_{1/2})$	1057.911 MHz	1059.271 MHz
$E(2p_{3/2})-E(2p_{1/2})$	10 969.03 MHz	10 972.02 MHz
$\Gamma(2p)$	$6.265\times10^8\,\text{sec}^{-1}$	$6.265\times10^8\,\text{sec}^{-1}$
α_{HFS} [a]	266.35 MHz	32.74 MHz

[a] The hyperfine-structure energy shifts are calculated from

$$\Delta E_{nljIF}=\frac{\alpha_{\text{HFS}}}{n^3}\left(\frac{F(F+1)-j(j+1)-I(I+1)}{j(j+1)(l+\frac{1}{2})}\right).$$

to the beam velocity in this run.[17] The dashed curve shows the theoretical prediction if hyperfine structure is disregarded. The time-dependent effect is a consequence of hyperfine structure and results from the slightly different depopulation rates of different hyperfine s states. Figure 5 demonstrates directly the effect of finite transit time. The two experimental points shown were obtained at the same quenching field of 151.6 V/cm but with different transit times resulting from different hydrogen-beam energies. The curve represents the theoretical prediction. These two points are statistically the most accurate single measurement ($\sim 3\times 10^7$ counts) and provide a precise test of the theory at moderately high field strengths. For the two transit times 19.9 and 31.4 nsec, the theoretical values of R are 0.151 02 and 0.151 78 while the experimental values are $0.150\,93 \pm 0.0002$ and $0.151\,72 \pm 0.0002$. The experimental values correspond to Lamb shifts of 1057.1 ± 1.6 and 1057.4 ± 1.6 MHz.

The extrapolated zero-field anisotropy in Fig. 4 is $0.139\,01 \pm 0.000\,12$ in good agreement with the theoretical value 0.139 078 including hyperfine-structure effects. (There is no time-dependent effect in the limit $\mathcal{F} \to 0$.) The value without hyperfine structure is 0.141 152. The uncertainty is that computed from the scatter in the individual measurements shown in Fig. 4. It is slightly smaller than what one would expect from counting statistics in a single measurement with the same total number of counts, indicating a high degree of stability over long-time periods. The zero-field polarization derived from Eq. (21) is -0.3229 ± 0.0003 compared with the theoretical value

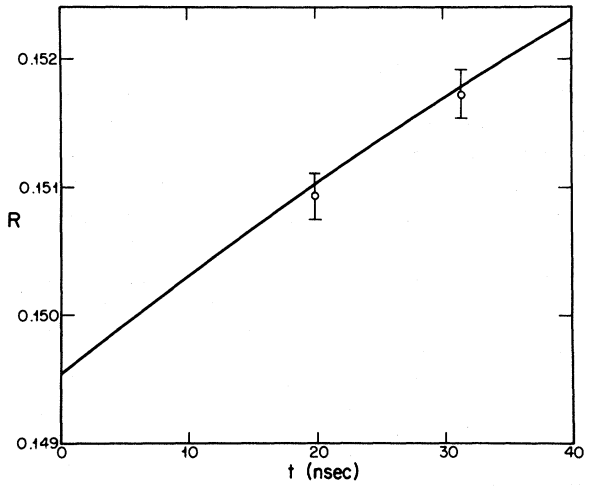

FIG. 5. Comparison of theoretical (solid curve) and experimental anisotropies for hydrogen as a function of elapsed time after entering the field of strength 151.6 V/cm.

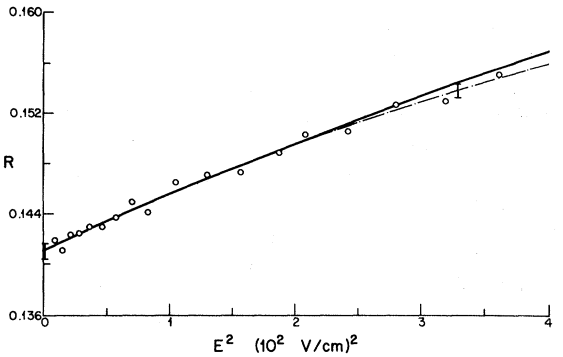

FIG. 6. Comparison of experimental and theoretical anisotropies for deuterium as a function of E^2. The dot-dash curve is the quadratic least-squares fit to the individual measurements shown by circles. The solid curve is the theory including hyperfine structure. The time-dependent effect shown in Fig. 4 for hydrogen is too small to be observable in deuterium.

0.323 090. It seems likely that the somewhat smaller value -0.30 ± 0.02 measured directly by Fite, Kauppila, and Ott[3] reflects an instrumental effect rather than a genuine disagreement with theory. The zero-field anisotropy corresponds to a Lamb shift of 1057.4 ± 1.0 MHz.

Figure 6 shows the results for metastable deuterium. Circles represent individual measurements; all have the same error shown by a single error bar. The dash-dot curve represents the quadratic least-squares fit and the solid curve is the theoretical calculation taking hyperfine structure and finite transit time into account. The effect of hyperfine structure and the consequent time dependence of R is much smaller because of the smaller coupling constant, but it has the effect of increasing the asymmetry. The zero-field value

TABLE VI. Summary of results.

Measurement	R_{expt}	R_{theor}	Δ_L (MHz)
	Hydrogen		
$R(\mathcal{F}\to 0)$	$0.139\,01 \pm 0.000\,12$	0.139 078	1057.4 ± 1.0
$R(\mathcal{F},t_1)$ [a]	$0.150\,93 \pm 0.0002$	0.151 02	1057.1 ± 1.6
$R(\mathcal{F},t_2)$ [a]	$0.151\,72 \pm 0.0002$	0.151 78	1057.4 ± 1.6
		Average	1057.3 ± 0.9
Microwave			1057.90 ± 0.06 [b] 1057.86 ± 0.06 [c]
	Deuterium		
$R(\mathcal{F}\to 0)$	$0.141\,21 \pm 0.000\,14$	0.141 30	1058.7 ± 1.1
Microwave			1059.28 ± 0.06 [d]

[a] $\mathcal{F} = 151.6$ V/cm, $t_1 = 19.9$ nsec, and $t_2 = 31.4$ nsec.
[b] Reference 9.
[c] S. Treibwasser, E. S. Dayhoff, and W. E. Lamb, Jr., Phys Rev. 89, 97 (1953).
[d] Reference 10.

is $0.141\,21 \pm 0.000\,14$ to be compared with the theoretical value 0.141 30. The corresponding Lamb shift is 1058.7 ± 1.1 MHz. The experimental results are summarized in Table VI.

The accuracy of the present results falls short of that obtained by microwave techniques by about an order of magnitude. However, the accuracy is still limited by counting statistics and a further improvement should not be difficult. There are several reasons mentioned in the Introduction which made the asymmetry method worthy of serious consideration as an alternative to the quench-rate method of determining Lamb shifts in heavy ($Z > 3$) hydrogenic ions. We have verified that the theory presented in this paper is valid to at least the $\pm 0.1\%$ level of accuracy. Experiments to improve the accuracy in hydrogen and extend the measurements to the ions are in preparation.

---

*Research supported by the National Research Council of Canada.

†Alfred P. Sloan Foundation Fellow.

‡Permanent address: Department of Physics, University of Edinburgh, Edinburgh, Scotland.

[1]G. W. F. Drake and R. B. Grimley, Phys. Rev. A 8, 157 (1973).

[2]A. van Wijngaarden, G. W. F. Drake, and P. S. Farago, Phys. Rev. Lett. 33, 4 (1974).

[3]W. L. Fite, W. E. Kauppila, and W. R. Ott, Phys. Rev. Lett. 20, 409 (1968); W. R. Ott, W. E. Kauppila, and W. L. Fite, Phys. Rev. A 1, 1089 (1970).

[4]I. A. Sellin, J. A. Biggerstaff, and P. M. Griffin, Phys. Rev. A 2, 423 (1970); G. Spiess, A. Valance, and P. Pradel, Phys. Rev. A 6, 746 (1972).

[5]C. Fan, M. Garcia-Munoz, and I. A. Sellin, Phys. Rev. 161, 6 (1967).

[6]H. W. Kugel, M. Leventhal, and D. E. Murnick, Phys. Rev. A 6, 1306 (1972).

[7]M. Leventhal, D. E. Murnick, and H. W. Kugel, Phys. Rev. Lett. 28, 1609 (1972).

[8]F. P. Lawrence, C. Y. Fan, and S. Bashkin, Phys. Rev. Lett. 28, 1612 (1972).

[9]R. Robiscoe and T. Shyn, Phys. Rev. Lett. 24, 559 (1970).

[10]B. Casens, Phys. Rev. 173, 49 (1968).

[11]G. W. F. Drake and R. B. Grimley, preceding paper [Phys. Rev. A 11, 1614 (1975)].

[12]P. R. Fontana and D. J. Lynch, Phys. Rev. A 2, 347 (1970).

[13]A. R. Edmonds, *Angular Momentum in Quantum Mechanics* (Princeton U. P., Princeton, N. J., 1957).

[14]J. W. Wooten and J. H. Macek, Phys. Rev. A 5, 137 (1972).

[15]A. S. Schlachter, P. J. Bjorkholm, D. H. Loyd, L. W. Anderson, and W. Haeberli, Phys. Rev. 177, 184 (1969).

[16]V. N. Tuan, G. Gautherin, and A. S. Schlachter, Phys. Rev. A 9, 1242 (1974).

[17]The field is not switched on suddenly, but rises gradually to its maximum value $\mathcal{F}_{max}$ over a distance of about 3.2 cm. The distance L from the quadrupole entrance slit to the center of the observation region is 4.32 cm. The effective interaction distance is estimated from the formula

$$L_{\text{eff}} = \int_0^L \mathcal{F}^2(x)\,dx/\mathcal{F}^2_{\text{max}},$$

giving $L_{\text{eff}} = 3.14$ cm. The effective interaction time is L_{eff}/v, where v is the beam velocity.